crystals

MDPI

Article

Efficient Continuous-Wave Eye-Safe Nd:$GdVO_4$/KGW Raman Laser and Sum Frequency Generation for Deep-Red Emission

Hsin-Jia Huang [1], Yu-Han Fang [1], Di Li [1], Chun-Ling Chen [1], Hsing-Chih Liang [2] and Yung-Fu Chen [1,*]

[1] Department of Electrophysics, National Yang Ming Chiao Tung University, Hsinchu 30010, Taiwan; peterhuang91.sc11@nycu.edu.tw (H.-J.H.); ann.sc11@nycu.edu.tw (Y.-H.F.); dili.sc09@nycu.edu.tw (D.L.); cjl310651070.sc10@nycu.edu.tw (C.-L.C.)

[2] Institute of Physics, National Yang Ming Chiao Tung University, Hsinchu 30010, Taiwan; hcliang@email.ntou.edu.tw

* Correspondence: yfchen@nycu.edu.tw

Abstract: A concise, efficient continuous-wave eye-safe Nd:$GdVO_4$/KGW Raman laser at 1525 nm is here demonstrated. A Nd:$GdVO_4$ crystal was used to produce the fundamental field at 1341 nm and a KGW crystal generated the intracavity Stokes field at 1525 nm via wavelength conversion of stimulated Raman scattering. The output power of the Stokes field at 1525 nm could achieve 2.1 W under the pump power of 30 W. Furthermore, two different lithium triborate (LBO) crystals with critical phase matching were exploited to obtain deep-red emission at 714 nm via the intracavity sum frequency generation of 1341 and 1525 nm waves. One cutting angle was in the XY plane and the other was in the XZ plane. The empirical thermo-optical coefficients for the LBO crystal were exploited to systematically analyze the critical phase matching conditions. Numerical results revealed that the type-I phase matching angle in the XY plane was near $\theta = 90°$ and $\phi = 3.3°$ at room temperature, whereas the type-I phase matching angle in the XZ plane was near $\theta = 86.3°$ and $\phi = 0°$ at a temperature around 47 °C. The numerical values for the optimal temperatures for the two different cutting angles were found to be in good agreement with experimental results. At the pump power of 30 W, the output power at 714 nm was approximately 2.9 W by using the LBO crystal with the cutting angle in the XY plane. On the other hand, the maximum output power at 714 nm could be up to 3.2 W under the pump power of 30 W by using the cutting angle in the XZ plane. Furthermore, the linewidth of the SFG emission was confirmed to be nearly the same for the two different cutting angles. The overall linewidth could be narrower than 0.2 nm. The developed laser at 714 nm can be useful in the exploration of ionic and atomic radium isotopes with laser spectroscopy.

Keywords: stimulated Raman scattering; continuous-wave laser; Nd:$GdVO_4$ crystal; eye-safe laser

Citation: Huang, H.-J.; Fang, Y.-H.; Li, D.; Chen, C.-L.; Liang, H.-C.; Chen, Y.-F. Efficient Continuous-Wave Eye-Safe Nd:$GdVO_4$/KGW Raman Laser and Sum Frequency Generation for Deep-Red Emission. *Crystals* **2023**, *13*, 1172. https://doi.org/10.3390/cryst13081172

Academic Editor: Sergei Smetanin

Received: 29 June 2023
Revised: 20 July 2023
Accepted: 26 July 2023
Published: 28 July 2023

1. Introduction

Light in the spectral range of 1.5–1.7 μm can be significantly absorbed by intraocular fluid and water in eye tissue so as not to wound the retina. On the other hand, lasers in the same wavelength range have excellent transparencies in the atmosphere and glass materials [1]. Due to the eye-safe property and atmospheric transparency, continuous-wave (CW) lasers in the 1.5–1.7 μm region have found increasing demand in medical applications and free space optical communications [2]. These applications require high brightness and high-power directed beams. Moreover, they are required in other applications such as supercontinuum generation using conventional silica fibers [3]. The approaches for achieving eye-safe lasers comprise direct emissions from solid-state lasers with active ions of Er^{3+}, Cr^{4+}, and Yb^{3+} [4–6] and nonlinear wavelength conversions from optical parametric oscillators (OPO) [7–9] or stimulated Raman scattering (SRS) [10–14]. Particularly, lasers based on intracavity SRS can provide beam quality improvement via Raman beam cleanup [15,16]. In comparison with the OPOs, Raman lasers are not constrained by the requirement of phase matching. Nowadays, eye-safe Raman lasers in the 1.5 μm region can

be obtained with the SRS crystals in the first Stokes line pumped by Nd-doped lasers at 1.3 μm from the $^4F_{3/2}\rightarrow{}^4I_{13/2}$ transition [17–19]. Since the stimulated emission of an Nd-doped laser at the $^4F_{3/2}\rightarrow{}^4I_{13/2}$ transition is significantly lower than that at the $^4F_{3/2}\rightarrow{}^4I_{11/2}$ transition, it is relatively difficult to generate CW solid-state Raman lasers near 1.5 μm from the first Stokes shift pumped by Nd-doped lasers at 1.3 μm. Consequently, eye-safe lasers based on SRS were almost developed with the Q-switched method. Quite recently, the first eye-safe Raman laser with CW operation was achieved by using composite laser crystal with in-band pumping [20]. CW dual-wavelength lasers at 1342 and 1525 nm were further developed by separating Nd:YVO_4 and YVO_4 crystals to concisely construct SRS cavities embedded in the fundamental wave resonator [21]. To our knowledge, CW eye-safe Raman lasers have never achieved output powers higher than 1.0 W.

Here, we give a brief synopsis of SRS to make this paper self-contained. When light encounters molecules in air, Rayleigh scattering is the dominant scattering mode, belonging to an elastic scattering. Rayleigh scattering that increases with the fourth power of frequency and is more effective at shorter wavelengths is the origin of the blue sky. On the other hand, incident photons may also interact with molecules, gaining or losing energy, leading to a change in the frequency of scattered photons. This inelastic scattering is called Raman scattering. Due to the increasing application in medicine, spectroscopy, defense, and general research, there is a great need for developing new sources of reliable, and preferably all-solid-state, laser radiation in hitherto uncovered spectral regions. SRS in solid-state crystals has been widely used for frequency conversion of laser radiation. Compared with gaseous and liquid Raman cells, the use of solid-state SRS converters has the advantages of higher conversion efficiency, no need for phase matching, and easier handling. The potassium gadolinium tungstate $KGd(WO_4)_2$ or KGW single crystal is a new and very promising Raman material for a wide range of pump pulse durations from picoseconds to nanoseconds [22,23]. Because of its low structure symmetry and high $\chi 3$-nonlinearity, KGW offers extremely rich advantages. KGW has a powerful Raman spectrum extending from ultraviolet to near infrared, so that it can be used for multiple applications. The crystal can be used as a reference material for Raman spectrum, as well as samples to study solid Raman scattering. In addition to being used as Raman crystals, KGW is also used in laser systems and used as a scintillator in medical imaging.

In this work, we achieved an efficient CW eye-safe Nd:$GdVO_4$/KGW Raman laser at 1525 nm with output power up to 2.1 W under the pump power of 30 W. The fundamental wave at 1341 nm was generated from the Nd:$GdVO_4$ crystal in the $^4F_{3/2}\rightarrow{}^4I_{13/2}$ transition. One end facet of the KGW Raman crystal was coated as an intracavity dichroic mirror to efficiently generate SRS in a separate cavity. The achievement of the wavelength conversion from 1341 to 1525 nm was furthermore exploited to develop a CW high-power laser at 714 nm via sum frequency generation (SFG). We employed lithium triborate crystals, known as LBO (LiB_3O_5), to perform the intracavity SFG. Two different cutting angles for the LBO crystals in the XY and XZ planes were designed to achieve the critical phase matching conditions. The empirical thermo-optical coefficients for the LBO crystal were systematically used to analyze the critical phase matching conditions. The type-I phase matching angle in the XY plane was numerically found to be near $\theta = 90^\circ$ and $\phi = 3.3^\circ$ at room temperature. On the other hand, the type-I phase matching angle in the XZ plane was calculated to be near $\theta = 86.3^\circ$ and $\phi = 0^\circ$ at a temperature around 47 °C. Experimental results revealed that the optimal temperatures of the LBO crystals for the two different cutting angles were in good agreement with numerical analyses. By using the LBO crystal with the cutting angle in the XY plane, the maximum output power at 714 nm was approximately 2.9 W at the pump power of 30 W. In contrast, the output power at 714 nm could reach 3.2 W by using the cutting angle in the XZ plane under the pump power of 30 W. Independent of the cutting angles, the linewidths for both deep-red emissions could be narrower than 0.2 nm. The developed laser at 714 nm is expected to be useful in the applications of laser spectroscopy [24,25].

2. Resonator Design and Experimental Configuration

The resonator setup for the diode-pumped Nd:$GdVO_4$/KGW Raman laser at 1525 nm in the CW operation is depicted in Figure 1. The pump source for the laser gain medium was a fiber-coupled diode laser at 808 nm with the maximum output power of 30 W, where the coupling fiber has a core diameter of 200 μm and a numerical aperture of 0.22. The input mirror was a concave mirror with a radius of curvature of 100 mm. The flat facet of the input mirror was coated to be antireflective (AR) at 808 nm (reflectance < 0.2%) and the concave facet was coated to be highly transmissive (HT) at 808 nm (transmittance > 95%) and highly reflective (HR) at 1341 nm (reflectance > 99.9%). The gain medium for the $^4F_{3/2} \rightarrow {}^4I_{13/2}$ transition at 1341 nm was an *a*-cut 0.25 at.% Nd:$GdVO_4$ crystal with a dimension of 3 × 3 × 15 mm^3. The Nd:$GdVO_4$ crystal was placed very close to the input mirror with a space of 1–2 mm. Both end facets of the Nd:$GdVO_4$ crystal were coated to be AR at the wavelengths of 808 and 1341 nm (reflectance < 0.2%). A N_p-cut KGW crystal with the dimension of 3 × 3 × 20 mm^3 was employed as the Raman gain medium. The polarization of the fundamental field was arranged to be parallel to the N_m axis of the KGW crystal to result in the strongest Raman shift at the wave number of 901 cm^{-1}. The first facet of the KGW crystal toward the Nd:$GdVO_4$ crystal was coated to be HT at 1341 nm (transmittance > 99.0%) and HR at 1525 nm (reflectance > 99.5%). Furthermore, the second facet of the KGW crystal was coated to be HT at 1341 and 1525 nm (transmittance > 99.0%) and HR at 714 nm (reflectance > 98%) for reflecting the backward SFG. Both the Nd:$GdVO_4$ and the KGW crystal were wrapped with indium foils and were mounted in water-cooled copper blocks with the temperature held at 20 °C. The output coupler was a concave mirror with a radius of curvature of 100 mm. To be brief, concave–concave and plano–concave cavities were used for the resonances of the fundamental and Stokes waves, respectively. The concave surface of the output coupler had a dichroic coating with HR at 1340 nm (reflectance > 99.9%) and a partial transmission at 1525 nm (transmittance = 0.5%) and HT at 714 nm (transmittance > 97%). The other surface of the output coupler was coated to be AR at 1525 and 714 nm (reflectance < 0.2%). The emission wavelength spectra were measured with an optical spectrum analyzer with a resolution of 0.1 nm (Advantest Q8381A).

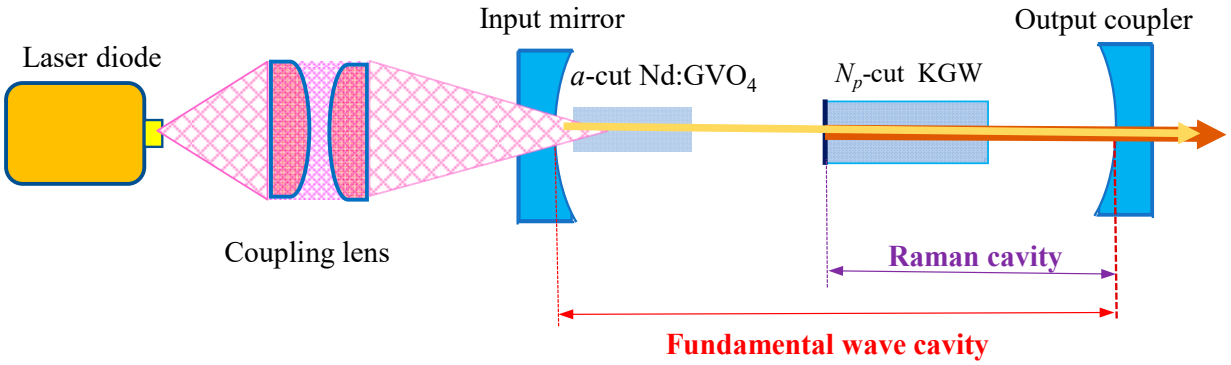

Figure 1. Resonator setup for the diode-end-pumped Nd:$GdVO_4$/KGW Raman laser at 1525 nm in the CW operation.

3. Experimental Results of Eye-Safe Emission at 1525 nm

Since the gain medium was placed near the input mirror, the cavity mode radius of the fundamental wave in the gain medium can be approximately expressed as [26]

$$\omega_1 = \left[\frac{\lambda_F L^*_{cav}}{\pi}\sqrt{\frac{g_2}{g_1(1-g_1g_2)}}\right]^{1/2}, \quad (1)$$

where λ_F is the wavelength of the fundamental wave, $g_1 = 1 - L^*_{cav}/R_1$, $g_2 = 1 - L^*_{cav}/R_2$, L^*_{cav} is the optical length of the laser cavity, and R_1 and R_2 are the radii of curvature for the input and output mirror, respectively. The optical length L^*_{cav} is given by

$$L^*_{cav} = L_{cav} - (1 - 1/n_G)\updownarrow_G - (1 - 1/n_K)\updownarrow_K, \quad (2)$$

where L_{cav} is the geometric length of the laser cavity, $\updownarrow_G$ and $\updownarrow_K$ are the lengths of the Nd:$GdVO_4$ and KGW, respectively, and n_G and n_K are the corresponding refractive indices. The geometric length L_{cav} was experimentally set to be 60 mm; consequently, the optical length L^*_{cav} was approximately 45 mm. The mirror facet of the KGW crystal was positioned at the beam waist of the fundamental wave for achieving the spatial overlap between the fundamental and Stokes fields. The mode radius of the fundamental beam waist is given by [26]

$$\omega_o = \left[\frac{\lambda_F L^*_{cav}}{\pi}\sqrt{\frac{g_1 g_2(1 - g_1 g_2)}{(g_1 + g_2 - 2g_1 g_2)^2}}\right]^{1/2}, \quad (3)$$

By substitution of L^*_{cav} = 45 mm and R_1 = R_2 = 100 mm into Equations (1) and (3), the values of ω_1 and ω_o could be calculated to be approximately 150 and 135 μm, respectively. The average pump radius was approximately 200 μm for achieving the mode matching between the pump and fundamental beams. From the cavity configuration shown in Figure 1, the cavity mode radius of the Stokes field at the mirror surface of KGW crystal can be given by

$$\omega_R = \left[\frac{\lambda_R}{\pi}\sqrt{L^*_{SRS}(R_2 - L^*_{SRS})}\right]^{1/2}, \quad (4)$$

where λ_R is the wavelength of the Stokes wave and L^*_{SRS} is the optical length of the SRS cavity. The optical length L^*_{SRS} can be given by $L^*_{SRS} = L_{SRS} - (1 - 1/n_K)\updownarrow_K$, where L_{SRS} is the geometric length of the SRS cavity. The geometric length L_{SRS} was set to be around 32 mm. From Equation (4), the optical length L^*_{SRS} can be calculated to be approximately 22 mm. The optical lengths L^*_{cav} and L^*_{SRS} satisfying the relation of $L^*_{cav} \approx 2L^*_{SRS}$ can be substituted into Equations (3) and (4) to confirm the spatial overlap between the fundamental and Stokes fields.

Experimental results for the fundamental, the Stokes, and the total output power versus the incident pump power are shown in Figure 2. The threshold pump powers for the fundamental and the Stokes emissions were approximately 1.6 W and 5.0 W, respectively. The output power for the fundamental emission at 1341 nm was found to initially increase with an increase in the pump power and gradually saturate for a pump power higher than 10 W. On the other hand, the output power of the Stokes emission at 1525 nm was found to linearly increase with an increase in the pump power. Under the maximum pump power of 30 W, the output power of the fundamental and the Stokes emissions were 0.3 and 2.1 W, respectively. For the CW Stokes 1.5 μm emission generated from the Nd-doped crystal 1.3 μm laser, the present conversion efficiency was considerably higher than the previous results [20,21]. The experimental result for the optical spectrum obtained at the pump power of 30 W is depicted in Figure 3. The Stokes emission at 1525 nm can be seen to dominate the output intensity. The beam quality M^2 factor for the laser output at 1525 nm was approximately 3.5 at the pump power of 30 W.

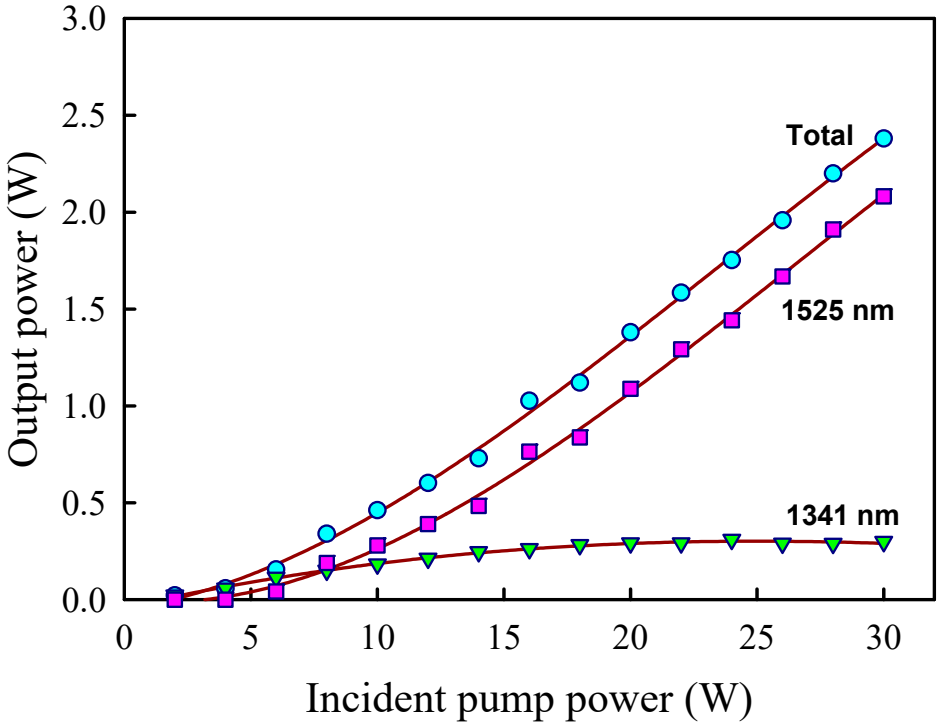

Figure 2. Experimental results for the fundamental, the Stokes, and the total output power versus the incident pump power.

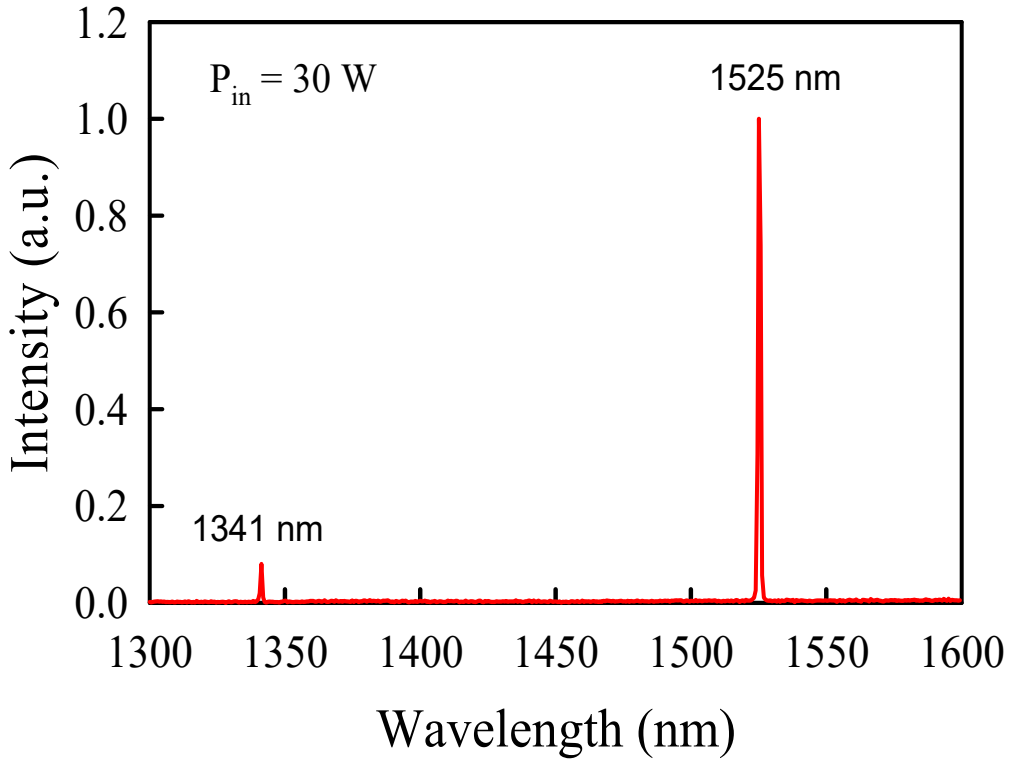

Figure 3. Experimental results for the optical spectrum measured at the pump power of 30 W.

4. Sum Frequency Generation for Deep-Red Emission

Based on the superior performance of the Stokes Raman generation, the laser cavity was further expanded to develop light emission at 714 nm by means of intracavity SFG, and the experimental setup is shown in Figure 4. We used two LBO crystals with different

cutting angles to make a comparison for the intracavity SFG of 1341 and 1525 nm. One cutting angle was in the XY plane and the other was in the XZ plane. The nonlinear optical properties of LBO crystal were thoroughly investigated by the Fujian Institute of Research on the Structure of Matter, Chinese Academy of Sciences. The high damage threshold of LBO crystals makes them very suitable for various wavelength conversions of high-intensity SHG and SFG in a wide spectrum. LBO crystal, belonging to an orthorhombic system with point group symmetry of mm^2, can achieve extremely high conversion efficiencies in nanosecond, picosecond, CW, and diode pumped Nd-doped laser systems for scientific, medical, industrial, and military applications. LBO is a negative biaxial crystal with unit cell dimensions of a = 8.4473 Å, b = 7.3788 Å, c = 5.1395 Å. The principal axes X, Y, and Z ($n_z > n_y > n_x$) of LBO crystal are parallel to the crystallographic axes a, c, and b, respectively. The temperature-dependent Sellmeier equations of n_x, n_y, and n_z for the LBO crystal can be given by [27]

$$n_x(\lambda, T) = \left(2.4542 + \frac{0.01125}{\lambda^2 - 0.01135} - 0.01388\lambda^2\right)^{1/2} + \frac{dn_x}{dT}(T - T_o), \quad (5)$$

$$n_y(\lambda, T) = \left(2.5390 + \frac{0.01277}{\lambda^2 - 0.01189} - 0.01848\lambda^2\right)^{1/2} + \frac{dn_y}{dT}(T - T_o), \quad (6)$$

$$n_z(\lambda, T) = \left(2.5865 + \frac{0.01310}{\lambda^2 - 0.01223} - 0.01861\lambda^2\right)^{1/2} + \frac{dn_z}{dT}(T - T_o), \quad (7)$$

where the units of wavelength λ are micrometers, the units of temperature T are degrees Celsius, and T_o = 20 °C. The three thermo-optical coefficients were provided by Velsko et al. in an earlier report [28]. Later, Tang et al. [29] experimentally explored the thermo-optical coefficients and modified them as

$$\frac{dn_x}{dT} = 2.0342 \times 10^{-7} - 1.9697 \times 10^{-8}T - 1.4415 \times 10^{-11}T^2, \quad (8)$$

$$\frac{dn_y}{dT} = -1.0748 \times 10^{-5} - 7.1034 \times 10^{-8}T - 5.7387 \times 10^{-11}T^2, \quad (9)$$

$$\frac{dn_z}{dT} = -8.5998 \times 10^{-7} - 1.5476 \times 10^{-7}T + 9.4675 \times 10^{-10}T^2 - 2.2375 \times 10^{-12}T^3, \quad (10)$$

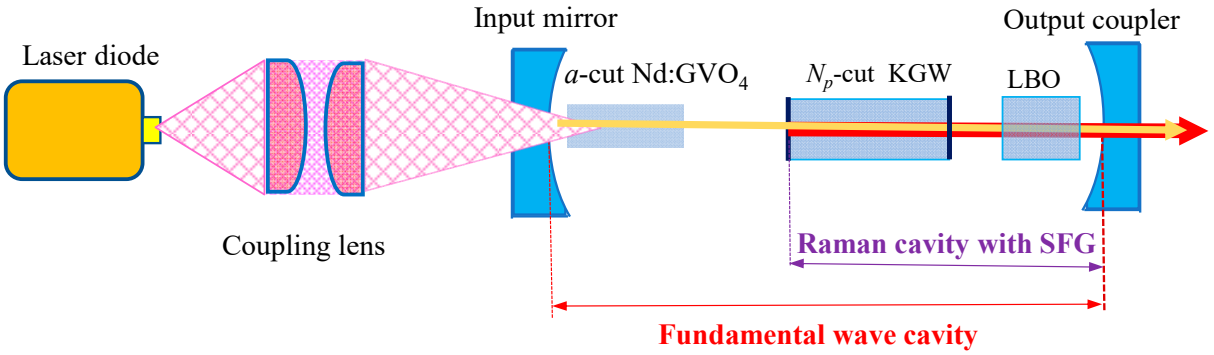

Figure 4. Experimental setup for the Nd:$GdVO_4$/KGW Raman laser with intracavity SFG.

The type-I phase matching in the XY plane of the LBO crystal is similar to that in the negative uniaxial crystal. The phase matching condition can be expressed as

$$\frac{n_z(\lambda_1, T)}{\lambda_1} + \frac{n_z(\lambda_2, T)}{\lambda_2} = \frac{n^e_{xy}(\lambda_3, T, \phi)}{\lambda_3}, \quad (11)$$

where $1/\lambda_1 + 1/\lambda_2 = 1/\lambda_3$ and the effective refractive index $n^e_{xy}(\lambda, T, \phi)$ is given by

$$n^e_{xy}(\lambda, T, \phi) = \left[\frac{\sin^2\phi}{n^2_x(\lambda, T)} + \frac{\cos^2\phi}{n^2_y(\lambda, T)}\right]^{-1/2}. \quad (12)$$

From Equations (5)–(10), the type-I phase matching angle in the XY plane can be found to be near $\theta = 90^\circ$ and $\phi = 3.3^\circ$ at room temperature. On the other hand, the type-I phase matching in the XZ plane of the LBO crystal is similar to that in the positive uniaxial crystal. The phase matching condition can be given by

$$\frac{n^o_{xz}(\lambda_1, T, \theta)}{\lambda_1} + \frac{n^o_{xz}(\lambda_2, T, \theta)}{\lambda_2} = \frac{n_y(\lambda_3, T)}{\lambda_3}, \quad (13)$$

where the effective refractive index $n^o_{xz}(\lambda, T, \theta)$ is given by

$$n^o_{xz}(\lambda, T, \theta) = \left[\frac{\cos^2\theta}{n^2_x(\lambda, T)} + \frac{\sin^2\phi}{n^2_z(\lambda, T)}\right]^{-1/2}. \quad (14)$$

From Equations (5)–(10), the type-I phase matching angle in the XZ plane can be found to be near $\theta = 86.3^\circ$ and $\phi = 0^\circ$ at a temperature around 47 °C. It is worthwhile to mention that the LBO crystal with the cutting angle along $\theta = 86.3^\circ$ and $\phi = 0^\circ$ can be also used for the SHG of 1341 nm at room temperature.

According to the analysis, we prepared two LBO crystals with the cutting angles satisfying the phase matchings in the XY and XZ planes, respectively. The dimensions of both LBO crystals were $3 \times 3 \times 8$ mm^3. In the experiment, we used an indium foil to wrap the LBO crystal, whose temperature was precisely controlled in the range of 20–60 °C by using a TEC-cooled holder. Both facets of the LBO crystal had an anti-reflective coating at 714, 1342, and 1525 nm (reflectance < 1.0%). The coating of the output coupler was designed to meet the requirement of HR within 1340–1530 nm (reflectivity > 99.9%) and HT at 714 nm (transmittance > 95%).

First of all, the LBO crystal with the cutting angle of $\theta = 90^\circ$ and $\phi = 3.3^\circ$ was used to explore the SFG performance. We experimentally observed the optimal temperature for the SFG output to be around 20 °C. This result was consistent with the numerical analysis. Figure 5 shows the experimental result for the SFG output power at 714 nm versus the pump power at 808 nm by using the LBO crystal with the cutting angle of $\theta = 90^\circ$ and $\phi = 3.3^\circ$ at the temperature of 20 °C. The output power at 714 nm could be seen to be approximately 2.9 W at the pump power of 30 W. In addition to the deep-red emission, the residual leakage power at 1341 and 1525 nm was found to be 0.71 W at the pump power of 30 W.

Next, the LBO crystal with the cutting angle of $\theta = 86.3^\circ$ and $\phi = 0^\circ$ was exploited to study the SFG performance. Based on thorough experimental results, the optimal temperature for the SFG output was found to be near 47 °C. Once again, the optimal temperature was in good agreement with the numerical calculation. Figure 6 shows the SFG output power at 714 nm versus the pump power at 808 nm by using the LBO crystal with the cutting angle of $\theta = 86.3^\circ$ and $\phi = 0^\circ$ at the temperature near 47 °C. It can be seen that the output power at the deep-red emission was up to 3.2 W at the pump power of 30 W. At the same time, the residual leakage power at 1341 and 1525 nm was approximately 0.62 W at the pump power of 30 W. In brief, the SFG output power attained with the LBO crystal with the phase matching in the XZ plane was approximately 10% higher than that in the XY plane. On the whole, the conversion efficiency obtained with KGW crystal as a Raman gain medium was significantly superior to the previous result obtained with YVO_4 crystal [30,31]. To the best of our knowledge, this is the highest output power of CW solid-state crystal Raman laser at 714 nm. It is worthwhile to mention that CW laser at 714 nm can be used as a pump source in the laser spectroscopy of atomic and ionic radium

isotopes [24,25]. Previously, a CW light source at 714 nm was usually developed with a Ti:sapphire CW ring laser.

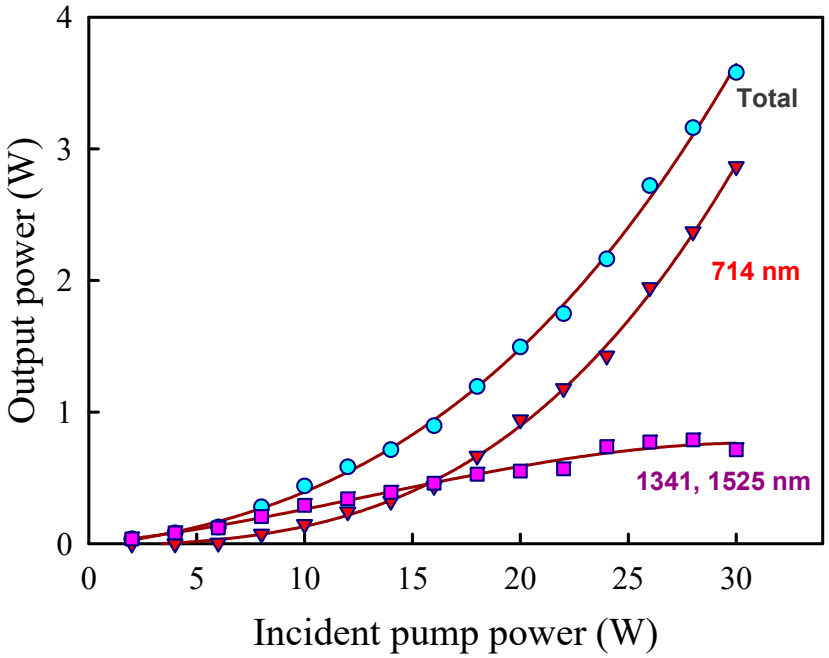

Figure 5. Experimental results for the SFG output power at 714 nm versus the pump power at 808 nm by using the LBO crystal with the cutting angle of $\theta = 90°$ and $\phi = 3.3°$ at room temperature.

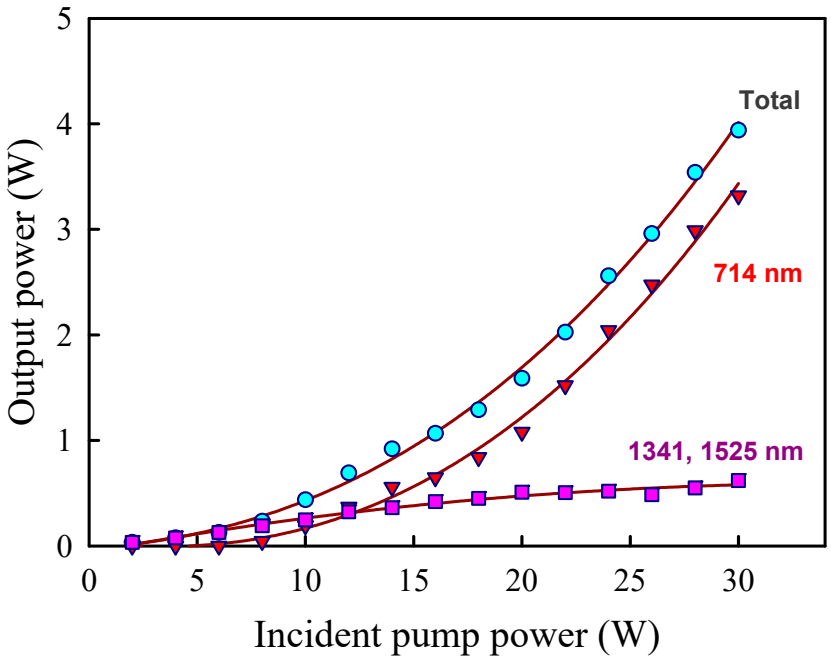

Figure 6. SFG output power at 714 nm versus pump power at 808 nm by using the LBO crystal with the cutting angle of $\theta = 86.3°$ and $\phi = 0°$ at a temperature around 47 °C.

Figure 7 shows the optical spectrum of the SFG output measured at the pump power of 30 W by using the LBO crystal with the cutting angle of $\theta = 86.3°$ and $\phi = 0°$. The overall linewidth of the SFG emission at 714 nm can be seen to be as narrow as 0.2 nm. There was no obvious difference in the linewidths of the deep-red emission obtained with two different LBO crystals. Again, there was little difference in the beam quality obtained

with the two different LBO crystals. The overall beam quality M^2 factor for the laser output at 714 nm was smaller than 2.5 at the pump power of 30 W, obviously better than that obtained for the emission at 1525 nm.

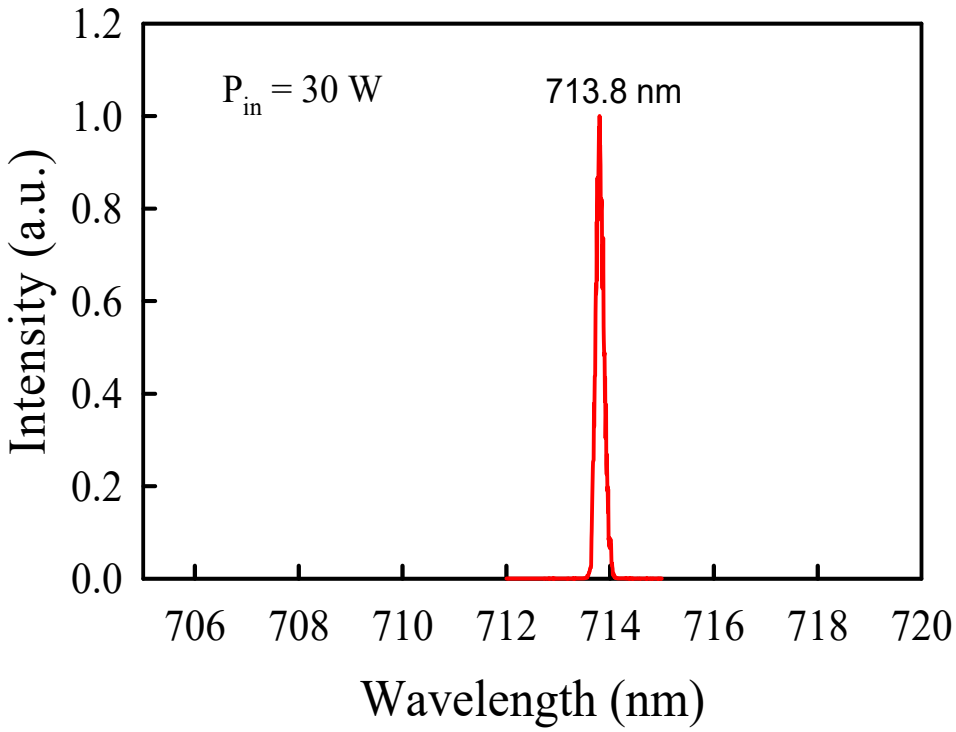

Figure 7. Optical spectrum of the SFG output measured at the pump power of 30 W.

5. Conclusions

In summary, we developed an efficient CW eye-safe Raman laser by using a Nd:$GdVO_4$ crystal as the gain medium for generating the fundamental wave at 1341 nm and a KGW crystal as the Raman gain medium for generating the Stokes wave at 1525 nm. At the pump power of 30 W, the maximum output power of the Stokes wave can be up to 2.1 W. Furthermore, we used two different LBO crystals with critical phase matching to achieve the intracavity SFG of the fundamental and Stokes waves. One cutting angle was in the XY plane and the other was in the XZ plane. We employed the empirical thermo-optical coefficients for the LBO crystal to systematically analyze the critical phase matching conditions. It was numerically found that the type-I phase matching angle in the XY plane was near $\theta = 90^\circ$ and $\phi = 3.3^\circ$ at room temperature, whereas the type-I phase matching angle in the XZ plane was near $\theta = 86.3^\circ$ and $\phi = 0^\circ$ at a temperature around 47 °C. The numerical values for the optimal temperatures for the two different cutting angles were confirmed to be in good agreement with experimental results. The maximum output power at 714 nm was approximately 2.9 W at the pump power of 30 W by using the LBO crystal with the cutting angle in the XY plane. On the other hand, the maximum output power at 714 nm under the pump power of 30 W could be up to 3.2 W by using the cutting angle in the XZ plane. Experimental results revealed that the linewidth of the SFG emission was nearly independent of the two different LBO crystals. The overall linewidth of the deep-red emission at 714 nm can be narrower than 0.2 nm. It is expected that the developed laser at 714 nm can be applied to the laser spectroscopy of atomic and ionic radium isotopes.

Author Contributions: Conceptualization, Y.-H.F. and Y.-F.C.; validation, D.L. and H.-J.H.; formal analysis, C.-L.C. and H.-C.L.; resources, Y.-H.F. and D.L.; writing—original draft preparation, Y.-F.C.; writing—review and editing, Y.-H.F., D.L., and Y.-F.C.; supervision, Y.-F.C. All authors have read and agreed to the published version of the manuscript.

Funding: This work is supported by the Ministry of Science and Technology of Taiwan (Contract No. 109-2119-M-009-015-MY3).

Data Availability Statement: Data underlying the results presented in this paper are not publicly available at this time but may be obtained from the authors upon reasonable request.

Conflicts of Interest: The authors declare no conflict of interest.

References

1. Tark, K.C.; Jung, J.E.; Song, S.Y. Superior lipolytic effect of the 1444 nm Nd:YAG Laser: Comparison with the 1064 nm Nd:YAG laser. *Lasers Surg. Med.* **2009**, *41*, 721–727. [CrossRef]
2. Hecht, J. Lidar for self-driving cars. *Opt. Photon. News* **2018**, *29*, 26–35. [CrossRef]
3. Abeeluck, A.K.; Headley, C.; Jorgensen, C.G. High-power supercontinuum generation in highly nonlinear, dispersion-shifted fibers by use of a continuous-wave Raman fiber laser. *Opt. Lett.* **2004**, *29*, 18. [CrossRef]
4. Sokólska, I.; Heumann, E.; Kück, S.; Łukasiewicz, T. Laser oscillation of Er^{3+}:YVO_4 and Er^{3+}, Yb^{3+}:YVO_4 crystals in the spectral range around 1.6 µm. *Appl. Phys. B* **2000**, *71*, 893. [CrossRef]
5. Sennaroglu, A. Broadly tunable Cr^{4+}-doped solid-state lasers in the near infrared and visible. *Prog. Quantum Electron.* **2002**, *26*, 287. [CrossRef]
6. Gorbachenya, K.N.; Kisel, V.E.; Yasukevich, A.S.; Maltsev, V.V.; Leonyuk, N.I.; Kuleshov, N.V. Highly efficient continuous-wave diode-pumped Er, Yb:$GdAl_3(BO_3)_4$ laser. *Opt. Lett.* **2013**, *38*, 2446. [CrossRef]
7. Huang, H.T.; He, J.L.; Liu, S.D.; Liu, F.Q.; Yang, X.Q.; Yang, H.W.; Yang, Y.; Yang, H. Synchronized generation of 1534nm and 1572nm by the mixed optical parameter oscillation. *Laser Phys. Lett.* **2011**, *8*, 358–362. [CrossRef]
8. Webb, M.S.; Moulton, P.F.; Kasinski, J.J.; Burnham, R.L.; Loiacono, G.; Stolzenberger, R. High-average-power $KTiOAsO_4$ optical parametric oscillator. *Opt. Lett.* **1998**, *23*, 1161. [CrossRef]
9. Chen, Y.F.; Chen, Y.C.; Chen, S.W.; Lan, Y.P. High-power efficient diode-pumped passively Q-switched Nd:YVO_4/KTP/Cr^{4+}:YAG eye-safe laser. *Opt. Commun.* **2004**, *234*, 337. [CrossRef]
10. Chen, Y.F. Compact efficient all-solid-state eye-safe laser with self-frequency Raman conversion in a Nd:YVO_4 crystal. *Opt. Lett.* **2004**, *29*, 2172. [CrossRef]
11. Ding, X.; Fan, C.; Sheng, Q.; Li, B.; Yu, X.; Zhang, G.; Sun, B.; Wu, L.; Zhang, H.; Liu, J.; et al. 5.2-W high-repetition-rate eye-safe laser at 1525 nm generated by Nd:YVO_4–YVO_4 stimulated Raman conversion. *Opt. Express* **2014**, *22*, 29121–29126. [CrossRef] [PubMed]
12. Yin, T.; Qi, Z.; Chen, F.; Song, Y.; He, S. High peak-power and narrow-linewidth all-fiber Raman nanosecond laser in 1.65 µm waveband. *Opt. Express* **2020**, *28*, 7175–7181. [CrossRef] [PubMed]
13. Chang, Y.T.; Su, K.W.; Chang, H.L.; Chen, Y.F. Compact efficient Q-switched eye-safe laser at 1525 nm with a double-end diffusion-bonded Nd:YVO_4 crystal as a self-Raman medium. *Opt. Express* **2009**, *17*, 4330–4335. [CrossRef] [PubMed]
14. Huang, J.; Lin, J.; Su, R.; Li, J.; Zheng, H.; Xu, C.; Shi, F.; Lin, Z.; Zhuang, J.; Zeng, W.; et al. Short pulse eye-safe laser with a stimulated Raman scattering self-conversion based on a Nd:KGW crystal. *Opt. Lett.* **2007**, *32*, 1096.
15. Murray, J.T.; Austin, W.L.; Powell, R.C. Intracavity Raman conversion and Raman beam cleanup. *Opt. Mater.* **1999**, *11*, 353–371. [CrossRef]
16. Reintjes, J.; Lehmberg, R.; Chang, R.; Duignan, M.; Calame, G. Beam cleanup with stimulated Raman scattering in the intensity-averaging regime. *J. Opt. Soc. Am. B* **1986**, *3*, 1408–1426. [CrossRef]
17. Chen, Y.F. Efficient 1521-nm Nd:$GdVO_4$ Raman laser. *Opt. Lett.* **2004**, *29*, 2632. [CrossRef]
18. Fan, Y.X.; Liu, Y.; Duan, Y.H.; Wang, Q.; Fan, L.; Wang, H.T.; Jia, G.H.; Tu, C.Y. High-efficiency eye-safe intracavity Raman laser at 1531 nm with SrWO4 crystal. *Appl. Phys. B* **2008**, *93*, 327. [CrossRef]
19. Shen, H.; Wang, Q.; Hu, W.; Chen, X.; Liu, Z.; Cong, Z.; Gao, L.; Tao, X.; Zhang, H.; Fang, J. Compact high repetition-rate actively Q-switched and mode-locked eye-safe Nd:$KLu(WO_4)_2$/$BaWO_4$ Raman laser. *Opt. Commun.* **2013**, *311*, 177. [CrossRef]
20. Fan, L.; Shen, J.; Wang, X.-Y.; Fan, H.-B.; Zhu, J.; Wang, X.-L.; Wang, H.-T. Efficient continuous-wave eye-safe Nd:YVO_4 self-Raman laser at 1.5 µm. *Opt. Lett.* **2021**, *46*, 3183–3186. [CrossRef]
21. Chen, Y.F.; Zheng, Z.X.; Huang, C.Y.; Guo, B.C.; Tsou, C.H.; Liang, H.C. Continuous wave dual-wavelength Nd:YVO_4 laser at 1342 and 1525 nm for generating a 714-nm emission. *Opt. Lett.* **2022**, *47*, 3792–3795. [CrossRef] [PubMed]
22. Lee, C.-C.; Huang, C.-Y.; Huang, H.-Y.; Chen, C.-M.; Tsou, C.-H. Comparison between Self-Raman Nd:YVO_4 Lasers and $NdYVO_4$/KGW Raman Lasers at Lime and Orange Wavelengths. *Appl. Sci.* **2021**, *11*, 11068. [CrossRef]
23. Ferreira, M.S.; Wetter, N.U. Yb:KGW self-Raman laser with 89 cm^{-1} Stokes shift and more than 32% diode-to-Stokes optical efficiency. *Opt. Laser Technol.* **2020**, *121*, 105835. [CrossRef]
24. Trimble, W.L.; Sulai, I.A.; Ahmad, I.; Bailey, K.; Graner, B.; Greene, J.P.; Holt, R.J.; Korsch, W.; Lu, Z.T.; Mueller, P.; et al. Lifetime of the 7s6d $^1D_2$ atomic state of radium. *Phys. Rev. A* **2009**, *80*, 054501. [CrossRef]
25. Booth, D.W.; Rabga, T.; Ready, R.; Bailey, K.G.; Bishof, M.; Dietrich, M.R.; Greene, J.P.; Mueller, P.; O'Connor, T.P.; Singh, J.T. Spectroscopic study and lifetime measurement of the 6d7p $^3F_2{}^o$ state of radium. *Spectrochim. Acta Part B* **2020**, *172*, 105967. [CrossRef]

26. Hodgson, N.; Weber, H. *Laser Resonators and Beam Propagation Fundamentals, Advanced Concepts and Applications*, 2nd ed.; Springer Series in Optical Sciences; Springer: New York, NY, USA, 2005.
27. Nikogosyan, D.N. *Nonlinear Optical Crystals: A Complete Survey*; Springer: Berlin, Germany, 2005.
28. Velsko, S.P.; Webb, M.; Davis, L.; Huang, C. Phase matched harmonic generation in lithium triborate (LBO). *IEEE J. Quantum Electron.* **1991**, *27*, 2182–2192. [CrossRef]
29. Tang, Y.; Cui, Y.; Dunn, M.H. Thermal dependence of the principal refractive indices of lithium triborate. *J. Opt. Soc. Am. B* **1995**, *12*, 638–643. [CrossRef]
30. Hsieh, C.L.; Huang, H.J.; Chen, C.L.; Liang, H.C.; Chen, Y.F. Selectable two-wavelength Nd:YVO_4 Raman laser at 671 and 714 nm. *Opt. Lett.* **2023**, *48*, 1510–1513. [CrossRef] [PubMed]
31. Huang, C.Y.; Guo, B.C.; Zheng, Z.X.; Tsou, C.H.; Liang, H.C.; Chen, Y.F. Continuous-Wave Crystalline Laser at 714 nm via Stimulated Raman Scattering and Sum Frequency Generation. *Crystals* **2022**, *12*, 1046. [CrossRef]